

# MultiSlice CAIPIRINHA Using View Angle Tilting Technique (CAIPIVAT)

Min-Oh Kim, Taehwa Hong, and Dong-Hyun Kim

Department of Electrical and Electronic Engineering, Yonsei University, Korea.

## Corresponding Author:

Dong-Hyun Kim, PhD

Department of Electrical and Electronic Engineering,

Yonsei University, Seoul, Korea;

E-mail: donghyunkim@yonsei.ac.kr

**Key Words:** simultaneous multislice imaging, field inhomogeneity artifact correction, CAIPIRINHA, view angle tilting

**Abbreviations:** Controlled aliasing in parallel imaging results in higher acceleration (CAIPIRINHA), view angle tilting (VAT), radiofrequency (RF), signal-to-noise ratio (SNR), simultaneous multislice (SMS), field-of-view (FOV), readout (RO), constrained least square (CLS), phase-encoding (PE), slice selection gradient ( $G_{ss}$ )

## ABSTRACT

We aim to focus on improving the performance of slice parallel imaging while simultaneously correcting for spatial shift artifacts related to off-resonance. In multislice controlled aliasing in parallel imaging results in higher acceleration (CAIPIRINHA), simultaneously excited slices are shifted along the phase-encoding direction by varying the radiofrequency phase for each slice, thereby obtaining virtually shifted coil sensitivity information. Meanwhile, the view angle tilting (VAT) technique provides additional shifts in the readout direction to further spread an image overlap while correcting for field inhomogeneity-induced spatial misregistration using a compensation gradient. By combining these features of CAIPIRINHA and VAT, named CAIPIVAT, the excited individual slices are shifted along both phase-encoding and readout directions. Consequently, the number of aliased voxels is reduced, and the virtual coil sensitivity information is more effectively used. Blurring due to the compensation gradient in VAT was alleviated by using a constrained least square filter. The advantages of CAIPIVAT are shown by signal-to-noise ratio simulation, phantom experiments, and in vivo experiments. Thus, CAIPIVAT can be useful for multislice parallel imaging while providing the correction of off-resonance-related spatial shift artifact.

## INTRODUCTION

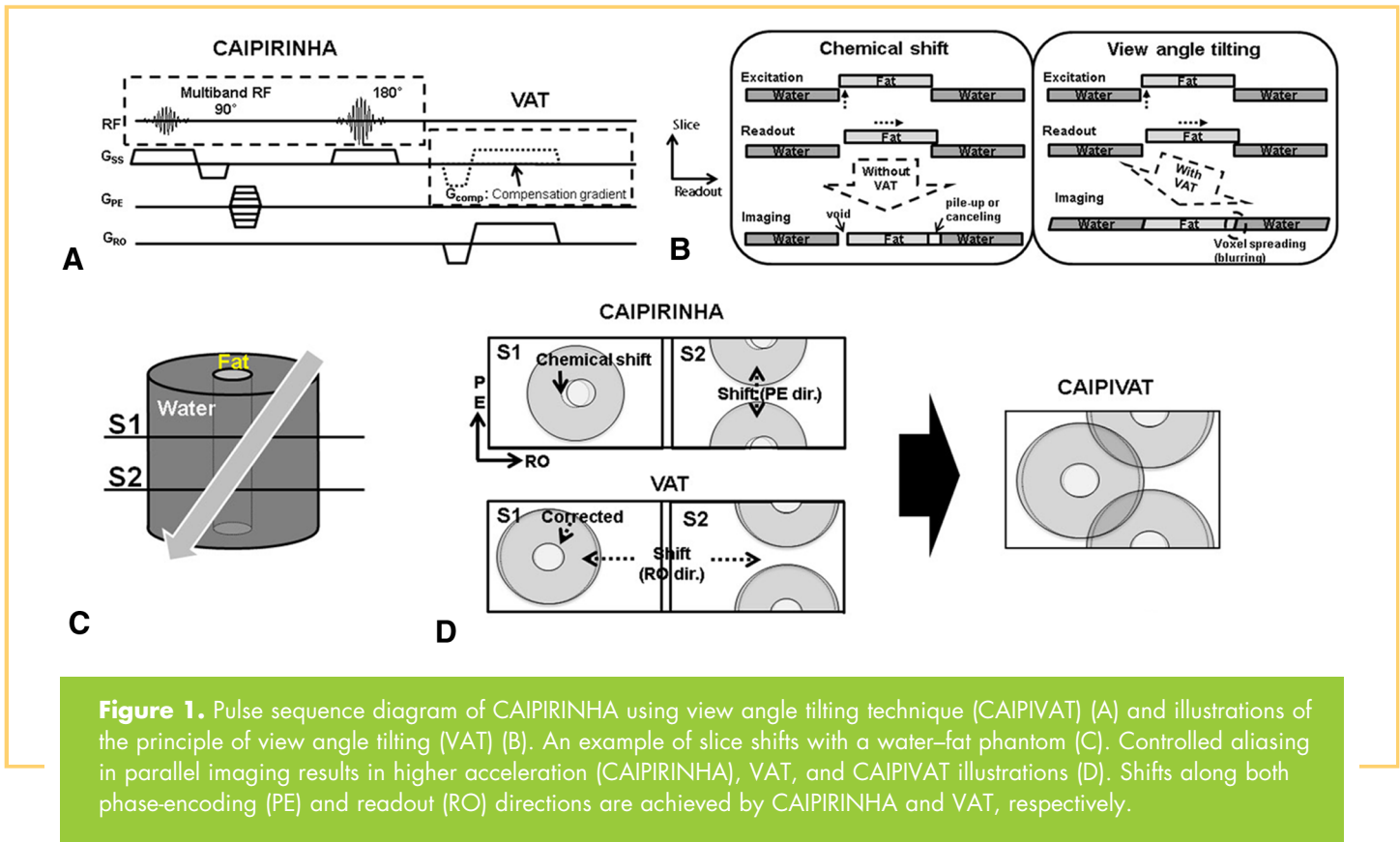
Reducing scan time is important for clinicians and patients, as well as for researchers. Various methods for reducing data acquisition time have been proposed and widely investigated. Data acquisition time can be directly reduced by using fast k-space sampling trajectory (1, 2) or undersampling (3, 4), which can result in aliasing artifact. There are many techniques for either resolving or separating this aliasing artifact in the context of parallel imaging using multichannel receiver coils (5, 6). In addition, data acquisition time efficiency can be improved when performing multislice imaging by simultaneous multislice (SMS) acquisitions, which collect signals from simultaneously excited regions along with increased data bandwidth acquisition (7, 8), controlling aliasing (9), multicoil arrays (10), or stepped B0 field method (11).

The SMS technique uses a multiband radiofrequency (RF) pulse to simultaneously excite several slices. In the early developmental stages of SMS, the excited multiple slices are separated into the frequency-encoding field of view (FOV) by applying an additional gradient along the slice direction during the readout (RO) time (7). The separated signals are acquired by increasing the total RO bandwidth. This concept has been successfully combined with the parallel imaging technique (12) and has been analyzed in a telecommunication

perspective in wideband magnetic resonance imaging (8, 13). These methods achieved through-plane acceleration. A similar gradient scheme can be found in the view angle tilting (VAT) technique (14, 15), where, in addition to the separation of multiple slices, chemical shift artifacts caused by excitation can be shifted back to their original position during RO. However, the additional gradient causes voxel shearing, which results in blurring as a tradeoff. The amount of blurring depends on the excitation slice profile and the strength of the applied gradients during the RO time.

Meanwhile, the simultaneously excited slices can be shifted along the phase-encoding (PE) direction by modifying the phase of the applied multiband RF pulse. In multislice controlled aliasing in parallel imaging results in higher acceleration (CAIPIRINHA) (9), aliased regions can be reduced and, consequently, the number of unfolding problems can also be reduced. In addition, slice-wise shifts make the sensitivity of each coil at individual slices more independent. While solving the slice-parallel imaging problem, its inverse problem can be better conditioned.

Here, we propose a strategy that combines the advantages of the multislice CAIPIRINHA and VAT techniques, termed CAIPIVAT. By applying the compensation gradient of VAT, a multislice shift along the RO direction can be achieved, whereas



field inhomogeneity-induced spatial shift can be corrected. The CAIPIRINHA makes each excited slice shift along the PE direction. Both PE and RO directional shifts can be accomplished; hence, the unfolding inverse problem becomes easy to solve. The inevitable blurring from the compensation gradient is addressed by implementing a deblurring technique, specifically a constrained least square (CLS) filter that is commonly used in digital image processing (16). The proposed method is shown using phantom and in vivo studies. Signal-to-noise ratio (SNR) gains of VAT, CAIPIRINHA, and CAIPIVAT are also simulated for assessing the effect of virtual coil sensitivity after solving the unfolding problem.

**METHOD**

The pulse sequence diagram is shown in Figure 1A. The multiband RF pulse was designed based on the Shinnar-Le Roux algorithm (17) to achieve the desired excitation profiles. A frequency modulation function for multiband excitation is defined according to the distance between the desired excitation slices ( $d_{slice}$ ). To induce the CAIPIRINHA shift along the PE direction, different RF phases were applied for each individual frequency band. The phase term of each band varied according to the number of bands and the amount of shift. This excitation profile affects the amount of blurring due to the VAT gradients; hence, it is crucial to apply a deblurring process that can improve the point spread function.

The aforementioned multiband scheme was combined with the VAT technique. VAT can correct off-resonance-related spatial shift artifacts by applying a compensation gradient during

the RO time. During the slice-selection process, the off-resonance spins are excited at a different position compared with the on-resonance spins. During RO, these off-resonance spins are encoded at a shifted location because of the off-resonance frequency term (Figure 1B, left). In the VAT technique, the off-resonance-related spatial shifts are corrected by projecting the excited spins along a specific view angle (Figure 1B, right). The amplitude of the compensation gradient ( $G_{comp}$ ) is set to be equal to that of the slice selection gradient ( $G_{SS}$ ). This  $G_{comp}$  can also be regarded as the separation gradient in SMS. The shift distance of each slice along the RO direction ( $d_{RO}$ ) depends on  $d_{slice}$  and the amplitude ratio between  $G_{comp}$  and  $G_{RO}$ , which is denoted as follows:

$$d_{RO} = d_{slice} \cdot \tan(G_{comp} / G_{RO}) \tag{1}$$

The signal equation of the VAT acquisition can be expressed as follows:

$$S(k_x, k_y, t) = \int_{z_0 - \frac{s}{2}}^{z_0 + \frac{s}{2}} \int_{x,y} m(x, y, z) \cdot e^{-j2\pi(xk_x(t) + yk_y + zk_z(t))} dx dy dz$$

$$= \text{sinc} \left( 2\pi k_x(t) \cdot R \cdot \frac{s}{2} \right) \cdot e^{-j2\pi k_x(t) \cdot R \cdot z_0} \cdot \int_{x,y} m(x, y) \cdot e^{-j2\pi(xk_x(t) + yk_y)} dx dy \tag{2}$$

where  $s$  is the slice thickness,  $z_0$  is the center of slice, and  $R$  represents  $G_{comp} / G_{RO}$ . The integration part along the  $z$ -direction can be expressed as the product of a sinc term and an exponential term (18). The exponential term is related to the off-reso-

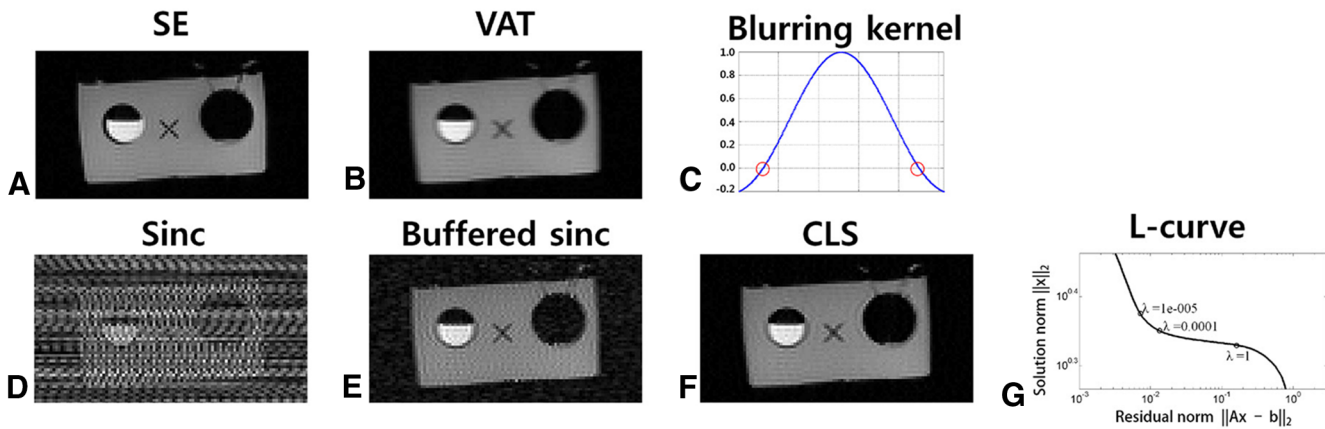


**Figure 2.** VAT blurring and its compensation. Reference SE image (A). Acquired VAT image (B). Blurring kernel (sinc function) and its zero crossing (red circle) (C). Deblurred image after direct demodulation of sinc (D). Deblurred image using buffered sinc, which excludes the near zero-crossing point (E). Deblurred image using the constrained least square (CLS) technique (F). L-curve for CLS filtering (G).

nance correction in VAT by shifting the off-resonance spins to its original position, and the sinc term is related to the VAT blurring (Figure 2B). In the k-space perspective, the acquired signal is modulated by a sinc function according to  $G_{comp}$ . Ideally, VAT blurring can be corrected (ie, deblurred) by simply demodulating this sinc function in k-space. However, this may cause a “divide by zero” problem because the sinc function can have zero-crossing points depending on the imaging parameter (Figure 2C). Thus, a direct sinc demodulation can cause noise amplification and degrade the image quality (Figure 2D). To avoid this unwanted noise amplification, the processing part of the singular point needs to be modified. As a simple approach, the values near the zero-crossing point can be thresholded such that no division is performed on these points (ie, buffered sinc). This method can avoid the ill-conditioning problem. However, division by the near-zero value still amplifies the noise. Here, the ill-conditioned deblurring process was rearranged as a constrained least square minimization problem as follows:

$$\min_{x_d} \|Ax_d - x_o\|^2 + \lambda \|R(x_d)\|^2 \quad (3)$$

where  $x_d$  is the desired deblurred image,  $x_o$  is the acquired VAT image,  $A$  is the sinc term in Equation 2 regarding the objective function,  $R(x_d)$  is the Laplacian image, and  $\lambda$  is a weighting factor for controlling the damping noise. The additional constraint can compensate for the zero-dividing problem. However, missing data points at zero crossings are not perfectly restored. The deblurring performance and noise amplification can be controlled by adjusting the weighting factor  $\lambda$ . The constrained least squares technique was tested on phantom data and adapted to CAPIVAT.

By combining CAPIRINHA and VAT, each slice shifts along both RO and PE directions depending on its slice direction position (Figure 1D). This feature can increase the reconstruction performance because the aliased regions are further reduced and the coil sensitivity of each slice retains more independency

again. In addition, the spatial shift artifacts related to off-resonance (eg, due to the chemical shift) can be mitigated by the VAT technique.

The expected SNR based on the g factor equation (9) was simulated for a 2-slice VAT, CAPIRINHA, and CAPIVAT acquisition assuming a cylindrical phantom. The in-plane diameter was set to be 80 mm, and the distance between the 2 slices varied from 1 to 50 mm. Simulations were conducted based on a 4-channel receiver coil assuming a variation of <10% for 50 mm along the slice direction. The view angle was set to 60°. The effects of VAT blurring were separately considered by examining the SNR after CLS filtering.

Experiments were performed on a 3 T scanner (Tim Trio, Siemens Medical Solutions, Erlangen, Germany) with a 12-channel, phased-array head coil. Three slices with a 9.0-mm gap were simultaneously excited, and a  $\pm$ FOV/3 shift was induced by the RF phase variation at each repetition time (TR). The imaging parameters are TR/echo time (TE) = 650.0/12.0 milliseconds, FOV = 192 × 96 mm<sup>2</sup> for the phantom experiments and 192 × 192 mm<sup>2</sup> for in vivo studies, resolution = 1.0 × 1.0 mm<sup>2</sup>, slice thickness = 2.0 mm, RO bandwidth = 390 Hz/pixel with a view angle of 63.1°, and total scan time = 62 seconds for phantom experiments and 125 seconds for in vivo studies. The phantom experiments were performed with a water-fat-air model for showing the capability of the chemical shift and the B0 artifact correction and for comparing the reconstruction performance between CAPIRINHA and CAPIVAT. In addition, in vivo head data were collected from a healthy volunteer to show the robustness to the chemical shift artifact and the acceleration. The study was approved by the institutional review board. Each data were reconstructed using slice-generalized autocalibrating partially parallel acquisitions (GRAPPA) technique (19), which resolves the aliased slices by calculating the GRAPPA kernel of each slice with a reference image information.

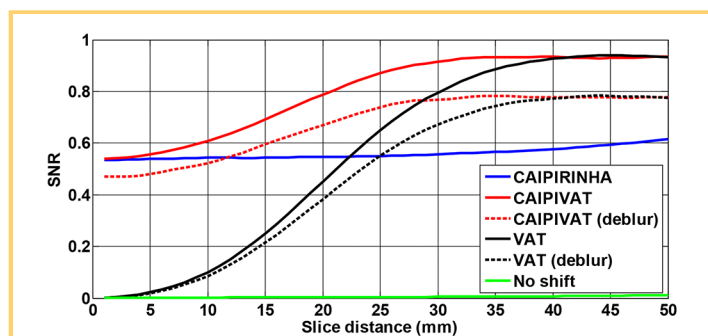


**Figure 3.** Signal-to-noise ratio (SNR) simulation for the case of a 2-slice imaging as a function of the slice distance. The SNRs of no-shift, VAT, VAT with deblurring, CAIPIVAT, CAIPIVAT with deblurring, and CAIPIRINHA are shown.

## RESULTS

Figure 3 shows the simulation result by presenting the effect of VAT shift and virtual coil sensitivity while solving the unfolding problem. According to the simulations, the “no shift” showed poor reconstruction performance because of the similar coil sensitivity along the slice direction. Likewise, CAIPIRINHA started at a higher SNR compared with the no-shift case, but it did not display much advantage as a function of the slice distance. CAIPIVAT, conversely, started at almost the same SNR compared with the CAIPIRINHA, as the effective VAT shift is near zero when the slice distance is small. However, as the slice distance increases, the SNR of CAIPIVAT also increased. Note that the SNR of VAT exceeded that of CAIPIRINHA after the 23-mm slice distance point. Furthermore, after approximately 46-mm separation, aliasing can be avoided using VAT only. Upon deblurring, the overall SNR in VAT and CAIPIVAT slightly reduced.

The CLS deblurring was tested on the phantom data. As shown in Figure 2, E and F, both buffered sinc and CLS filter can alleviate VAT blurring better than direct demodulation of the sinc function. Between these 2 methods, the image quality is highly improved in the result image using CLS filter, particularly on the noise components. However, a ringing artifact was observed because of missing data at the zero-crossing points in the sinc function.

Using the water-fat-air model phantom, field inhomogeneity-induced spatial shifts, which appeared as a slight signal pile up at the air-water interface, and chemical shift artifact due to oil are corrected in CAIPIVAT acquisition as shown in Figure 4. Furthermore, comparing the acquired images with CAIPIRINHA and CAIPIVAT, the aliased regions are considerably reduced in CAIPIVAT, and, consequently, this property makes the unfolding problems easy to solve. Signal decrement after CAIPIRINHA reconstruction was observed in slice 2. In in vivo imaging (Figure 5), the spatial shift due to chemical shifts of the fatty tissue around the skull was corrected in CAIPIVAT, and it showed less parallel imaging artifact.

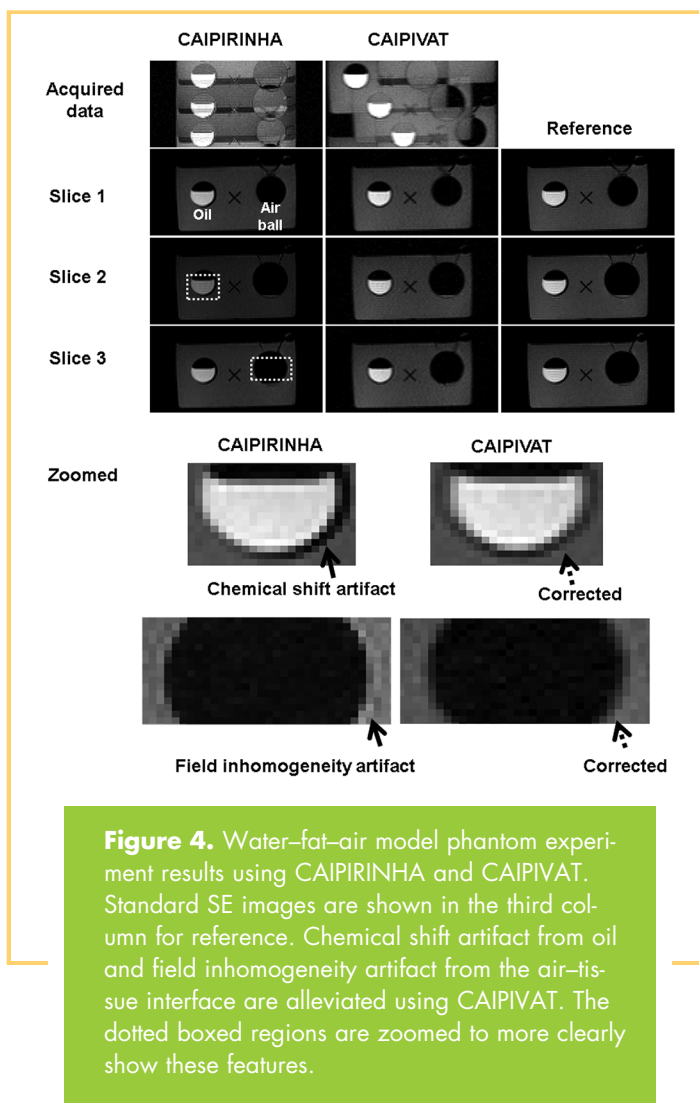


**Figure 4.** Water-fat-air model phantom experiment results using CAIPIRINHA and CAIPIVAT. Standard SE images are shown in the third column for reference. Chemical shift artifact from oil and field inhomogeneity artifact from the air-tissue interface are alleviated using CAIPIVAT. The dotted boxed regions are zoomed to more clearly show these features.

## DISCUSSION

With the CAIPIVAT technique, the number of voxels to solve the unfolding problem is reduced more compared with that of aliased voxels of CAIPIRINHA because of the in-plane shifts along both the PE and RO directions. Furthermore, ill-conditioned problems due to the similar coil sensitivity of each slice can be better conditioned by obtaining the independence (reducing the similarity) of virtual coil sensitivities. These features result in reducing the g factor as shown in the simulation result and give a chance to increase the multislice excitation factor. Recently, a general formalism of CAIPIRINHA, named wave-CAIPI, which controls aliasing in arbitrary directions, was introduced (20, 21). CAIPIVAT can be considered to fall into the category of SMS wave-CAIPI.

Moreover, the VAT technique has the ability to compensate off-resonance-related spatial shift artifacts by matching  $G_{SS}$  and  $G_{comp}$ . The view angle of 60–65°, which was used here, is determined by the imaging parameters (slice thickness, RF bandwidth, RO bandwidth, and resolution). Different view angles can be used by changing these imaging parameters if needed. For example, a wider separation of the multislice images may be desired by increasing the view angle. In this case, the ability to

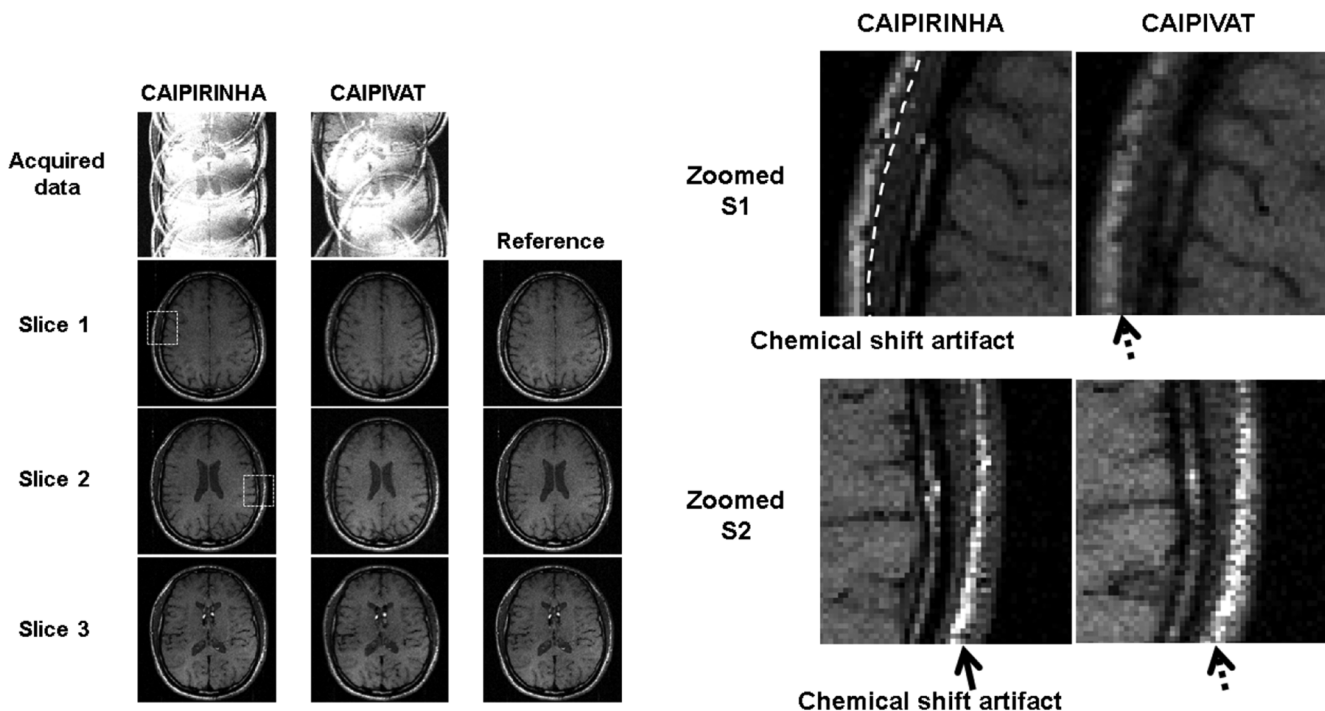


**Figure 5.** In vivo brain experiment results using CAIPIRINHA and CAIPIVAT. Standard SE images are shown in the third column for reference. Chemical shift artifacts at skull bone and scalp are alleviated using CAIPIVAT. The dotted boxed regions are zoomed to more clearly show these features. In the zoomed slice 1, signal void due to the chemical shift is indicated by a dotted white line, and its corrected version is indicated by a dotted black arrow.

correct the spatial shift remains the same; however, the overall blurring would be different. This blurring can be alleviated by using the deblurring CLS technique.

In general, the appropriate number of simultaneous multislice factors depends on the receiver coils and imaging parameters. In other words, the number of receiver coils, the geometric distribution of their sensitivities, volume coverage, and slice gap are important in deciding the multiband factor. Furthermore, here, the number of shifts should be carefully considered because the coil sensitivities are virtually shifted along both the PE and RO directions. If the virtually shifted coil sensitivities happen to be similar at the aliased regions, the reconstructed image may have poor SNR.

Although the number of simultaneously excited slices can be increased by adding the modulated RF pulses, in reality, this increase is limited because of the peak power of RF, which increases

proportional to the number of slices in a simple multiband RF design scheme. To increase the number of excitation bands, a special technique is required such as variable-rate selective excitation (22) or power independent of number of slices (23) because the peak RF power increases proportional to the number of slices in the simple multiband RF design scheme. These advanced multiband RF design schemes are essential, particularly in selective  $180^\circ$  RF pulses in SE-based sequences.

In conclusion, we presented a CAIPIVAT technique for SMS imaging with inherent spatial shift artifact correction due to field inhomogeneity. A constrained reconstruction was used to alleviate the problem of blurring in VAT-based acquisitions. This technique can be useful for reducing data acquisition time in slice-encoding metal artifact correction (24) that involves VAT for correcting in-plane field inhomogeneity artifacts.

## REFERENCES

1. Irrazabal P, Nishimura DG. Fast three dimensional magnetic resonance imaging. *Magn Reson Med.* 1995;33(5):656–662.
2. Spielman DM, Pauly JM, Meyer CH. Magnetic resonance fluoroscopy using spirals with variable sampling densities. *Magn Reson Med.* 1995;34(3):388–394.
3. Feinberg DA, Hale JD, Watts JC, Kaufman L, Mark A. Halving MR imaging time by conjugation: demonstration at 3.5 kG. *Radiology.* 1986;161(2):527–531.
4. Sodickson DK, Manning WJ. Simultaneous acquisition of spatial harmonics (SMASH): fast imaging with radiofrequency coil arrays. *Magn Reson Med.* 1997; 38(4):591–603.
5. Pruessmann KP, Weiger M, Scheidegger MB, Boesiger P. SENSE: sensitivity encoding for fast MRI. *Magn Reson Med.* 1999;42(5):952–962.
6. Griswold MA, Jakob PM, Heidemann RM, Niitka M, Jellus V, Wang J, Kiefer B, Haase A. Generalized autocalibrating partially parallel acquisitions (GRAPPA). *Magn Reson Med.* 2002;47(6):1202–1210.
7. Weaver JB. Simultaneous multislice acquisition of MR images. *Magn Reson Med.* 1988;8(3):275–284.
8. Wu EL, Chen JH, Chiueh TD. Wideband MRI: theoretical analysis and its applications. *Conf Proc IEEE Eng Med Biol Soc.* 2010;2010:5681–5684.
9. Breuer FA, Blaimer M, Heidemann RM, Mueller MF, Griswold MA, Jakob PM. Controlled aliasing in parallel imaging results in higher acceleration (CAIPIRINHA) for multi-slice imaging. *Magn Reson Med.* 2005;53(3):684–691.
10. Larkman DJ, Hajnal JV, Herlihy AH, Coutts GA, Young IR, Ehnholm G. Use of multicoil arrays for separation of signal from multiple slices simultaneously excited. *J Magn Reson Imaging.* 2001;13(2):313–317.
11. Paley MN, Lee KJ, Wild JM, Fichte S, Whitby EH, Wilkinson ID, Van Beek EJ, Griffiths PD. B1AC-MAMBA: B1 array combined with multiple-acquisition micro B0 array parallel magnetic resonance imaging. *Magn Reson Med.* 2003;49(6): 1196–1200.

12. Paley MN, Lee KJ, Wild JM, Griffiths PD, Whitby EH. Simultaneous parallel inclined readout image technique. *Magn Reson Imaging*. 2006;24(5):557–562.
13. Kim MO, Lee J, Zho SY, Kim DH. Accelerated MR whole brain imaging with sheared voxel imaging using aliasing separation gradients. *Med Phys*. 2013;40(6):062301.
14. Cho ZH, Kim DJ, Kim YK. Total inhomogeneity correction including chemical shifts and susceptibility by view angle tilting. *Med Phys*. 1988;15(1):7–11.
15. Kim MO, Zho SY, Kim DH. 3D imaging using magnetic resonance tomosynthesis (MRT) technique. *Med Phys*. 2012;39(8):4733–4741.
16. Hunt BR. The application of constrained least squares estimation to image restoration by digital computer. *IEEE Trans Comput*. 1973;22(9):805–812.
17. Pauly J, Le Roux P, Nishimura D, Macovski A. Parameter relations for the Shinnar-Le Roux selective excitation pulse design algorithm [NMR imaging]. *IEEE Trans Med Imaging*. 1991;10(1):53–65.
18. Butts K, Pauly JM, Gold GE. Reduction of blurring in view angle tilting MRI. *Magn Reson Med*. 2005;53(2):418–424.
19. Setsompop K, Gagoski BA, Polimeni JR, Witzel T, Wedeen VJ, Wald LL. Blipped-controlled aliasing in parallel imaging for simultaneous multislice echo planar imaging with reduced g-factor penalty. *Magn Reson Med*. 2012;67(5):1210–1224.
20. Bilgic B, Gagoski BA, Cauley SF, Fan AP, Polimeni JR, Grant PE, Wald LL, Setsompop K. Wave-CAIPI for highly accelerated 3D imaging. *Magn Reson Med*. 2015;73(6):2152–2162.
21. Gagoski BA, Bilgic B, Eichner C, Bhat H, Grant PE, Wald LL, Setsompop K. RARE/turbo spin echo imaging with simultaneous multislice Wave-CAIPI. *Magn Reson Med*. 2015;73(3):929–938.
22. Hargreaves BA, Cunningham CH, Nishimura DG, Conolly SM. Variable-rate selective excitation for rapid MRI sequences. *Magn Reson Med*. 2004;52(3):590–597.
23. Norris DG, Koopmans PJ, Boyacioglu R, Barth M. Power Independent of Number of Slices (PINS) radiofrequency pulses for low-power simultaneous multislice excitation. *Magn Reson Med*. 2011;66(5):1234–1240.
24. Lu W, Pauly KB, Gold GE, Pauly JM, Hargreaves BA. SEMAC: Slice Encoding for Metal Artifact Correction in MRI. *Magn Reson Med*. 2009;62(1):66–76.